

# Synthesis, Structural Characterization, and Luminescent Properties of Heteroleptic Bismuth-Organic Compounds

*Alyssa K. Adcock, Alexander C. Marwitz, Lulio Sanz, R. Lee Ayscue III, Jeffery A. Bertke, and  
Karah E. Knope\**

Department of Chemistry, Georgetown University, 37th and O Streets, NW, Washington, D.C.  
20057, USA

## Supporting Information

Crystallographic Refinement Details.....	2
Powder X-Ray Diffraction Patterns.....	6
Raman Spectra .....	11
Thermogravimetric Analysis .....	14
Luminescence Measurements .....	19
Summary of Potential Hydrogen Bonding Interactions in <b>1-6</b> . .....	25

## Crystallographic Refinement Details

### $\text{Bi}_2(\text{terpy})_2(\text{MeO})_2(\text{NO}_3)_4$ (1)

All H atoms were included as riding idealized contributors; H atom U's were assigned as 1.2 times carrier  $U_{\text{eq}}$ .

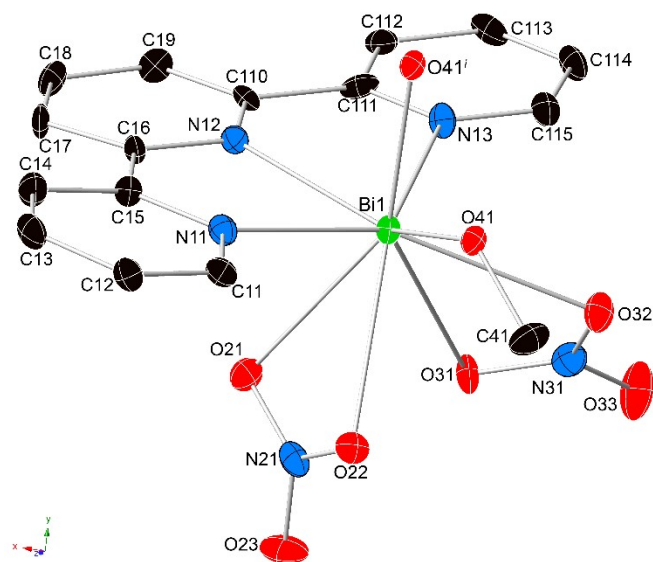


**Figure S1.** Thermal ellipsoid plot of **1**. Ellipsoids are shown at 50% probability. Symmetry operators: (i)  $-x+1, -y+1, -z+1$ .

### $\text{BiNO}_3(\text{TTA})_2(\text{terpy})$ (2)

The thiophene ring portion of each TTA ligand is disordered over two orientations. The ratio of Part A to Part B for the first TTA ligand ( $\text{C}25 > \text{S}21$ ) refines to 0.75, while the other ( $\text{C}35 > \text{S}31$ ) refines to 0.45. One F atom (F33) is disordered over two positions, with the ratio of Part A to Part B equal to 0.68. The like S-C and C-C bonds have been restrained to be similar. Similar displacement amplitudes were imposed on disordered sites overlapping by less than the sum of van der Waals radii. All H atoms were included as riding idealized contributors; H atom U's were assigned as 1.2 times carrier  $U_{\text{eq}}$ .

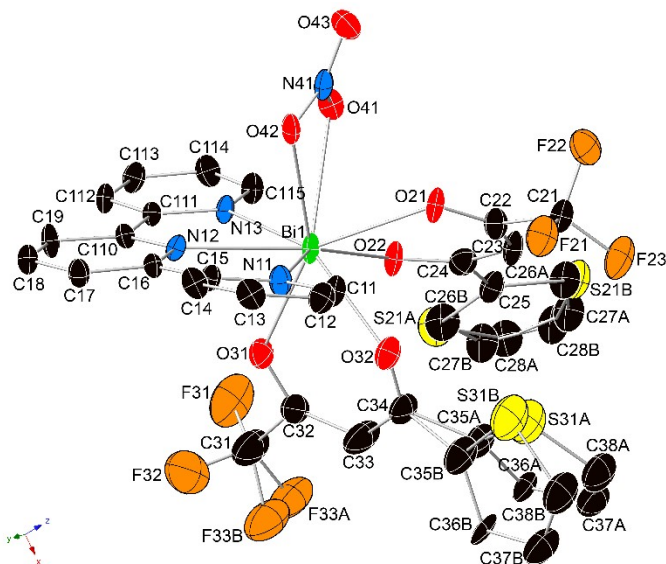


**Figure S2.** Thermal ellipsoid plot of **2**. Ellipsoids are shown at 50% probability.

### **BiCl(TTA)<sub>2</sub>(terpy) (3)**

The thiophene ring portion of each TTA ligand is disordered over two orientations. The ratio of Part A to Part B for the first TTA ligand (C12>S11) refines to 0.62, while the other (C25>S21) refines to 0.93. The like S-C and C-C bonds have been restrained to be similar. Similar displacement amplitudes were imposed on disordered sites overlapping by less than the sum of van der Waals radii. All H atoms were included as riding idealized contributors; H atom U's were assigned as 1.2 times carrier  $U_{eq}$ .

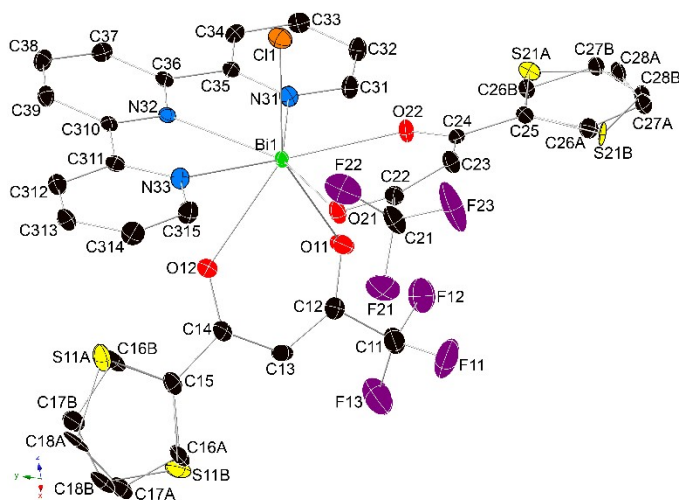


**Figure S3.** Thermal ellipsoid plot of **3**. Ellipsoids are shown at 50% probability.

### **BiBr(TTA)<sub>2</sub>(terpy) (4)**

The thiophene ring portion (C25>S21) of one TTA ligands is disordered over two orientations, where the ratio of Part A to Part B refines to 0.63. The like S-C and C-C bonds have been restrained

to be similar. Similar displacement amplitudes were imposed on disordered sites overlapping by less than the sum of van der Waals radii. The three most disagreeable reflections were likely affected by the beamstop and therefore, omitted. All H atoms were included as riding idealized contributors; H atom U's were assigned as 1.2 times carrier  $U_{eq}$ .

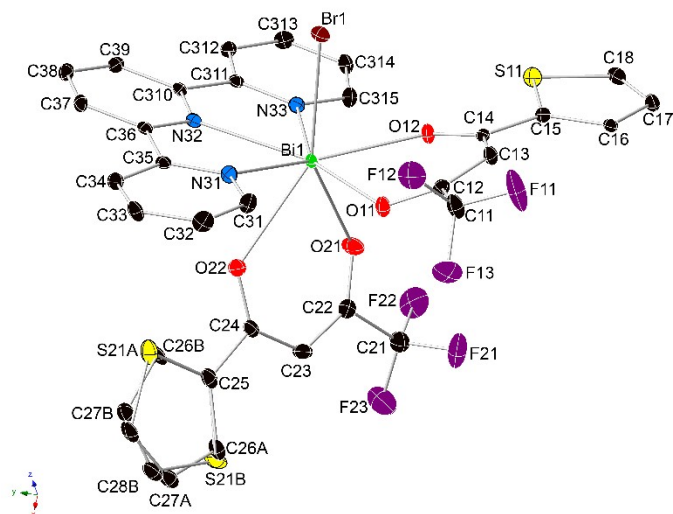


**Figure S4.** Thermal ellipsoid plot of **4**. Ellipsoids are shown at 50% probability.

### **BiBr<sub>2</sub>(TTA)(terpy) (5)**

The most disagreeable reflection (002) was likely affected by the beamstop, and as such, omitted. All H atoms were included as riding idealized contributors; H atom U's were assigned as 1.2 times carrier  $U_{eq}$ .

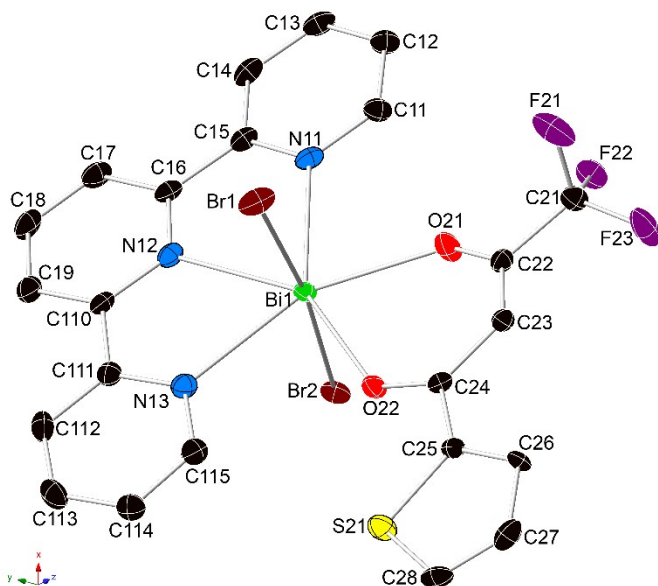


**Figure S5.** Thermal ellipsoid plot of **5**. Ellipsoids are shown at 50% probability.

### EuNO<sub>3</sub>(TTA)<sub>2</sub>(terpy) (6)

The thiophene ring portion of one TTA ligand is disordered over two orientations. The ratio of Part A to Part B for the TTA ligand (C25>S21) refines to 0.50. The like S-C and C-C bonds have been restrained to be similar. Similar displacement amplitudes were imposed on disordered sites overlapping by less than the sum of van der Waals radii. All H atoms were included as riding idealized contributors; H atom U's were assigned as 1.2 times carrier U<sub>eq</sub>.

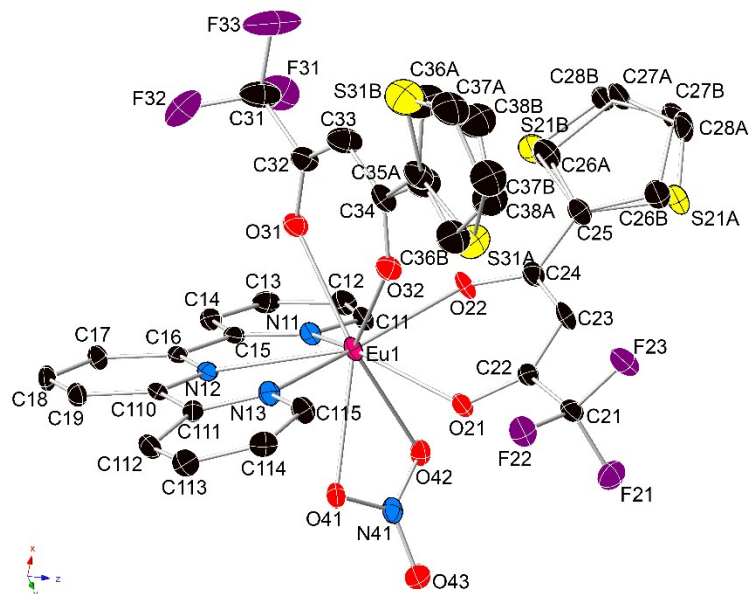


**Figure S6.** Thermal ellipsoid plot of **6**. Ellipsoids are shown at 50% probability.

## Powder X-Ray Diffraction Patterns

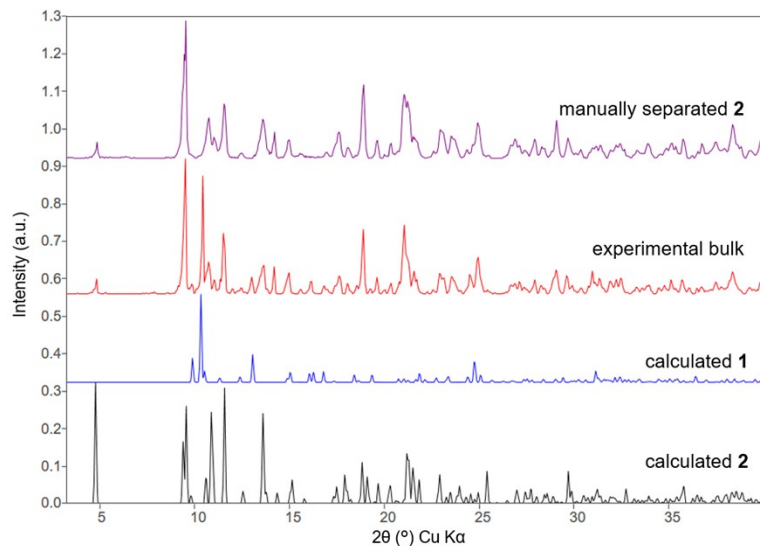


**Figure S7.** Powder X-ray diffraction data for the bulk product from which **1** and **2** were isolated. Agreement between the calculated pattern and observed pattern of the manually separated powder pattern of **2** indicates that the crystal used for structural determination is representation of the bulk, as confirmed by element analysis.

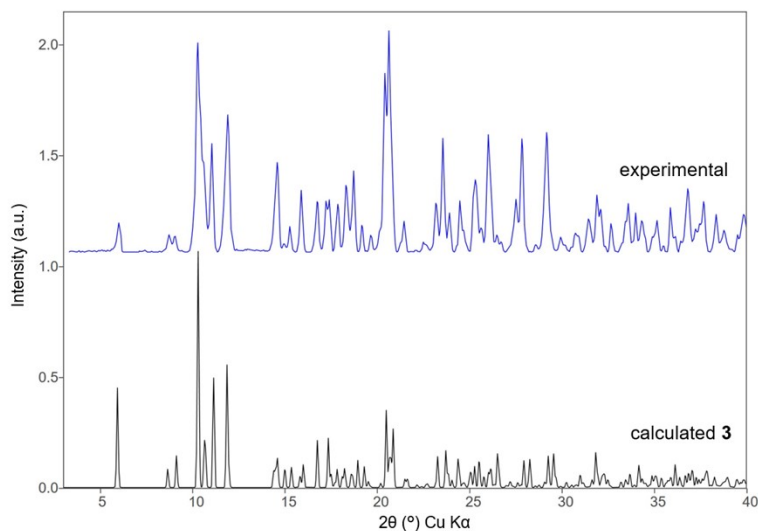


**Figure S8.** Powder X-ray diffraction data for the bulk product from which **3** was isolated. Agreement between the calculated pattern and observed pattern indicates that the crystal used for structural determination is representation of the bulk, as confirmed by element analysis.

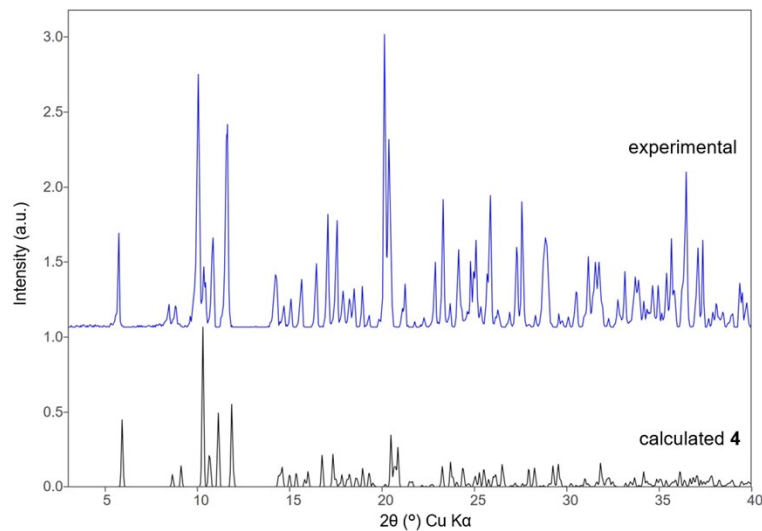


**Figure S9.** Powder X-ray diffraction data for the bulk product from which **4** was isolated. Agreement between the calculated pattern and observed pattern indicates that the crystal used for structural determination is representation of the bulk, as confirmed by element analysis.

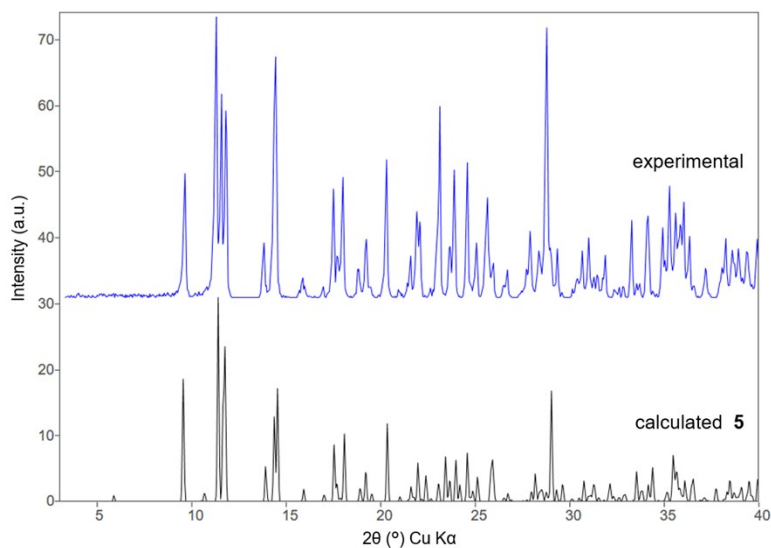


**Figure S10.** Powder X-ray diffraction data for the bulk product from which **5** was isolated. Agreement between the calculated pattern and observed pattern indicates that the crystal used for structural determination is representation of the bulk, as confirmed by element analysis.

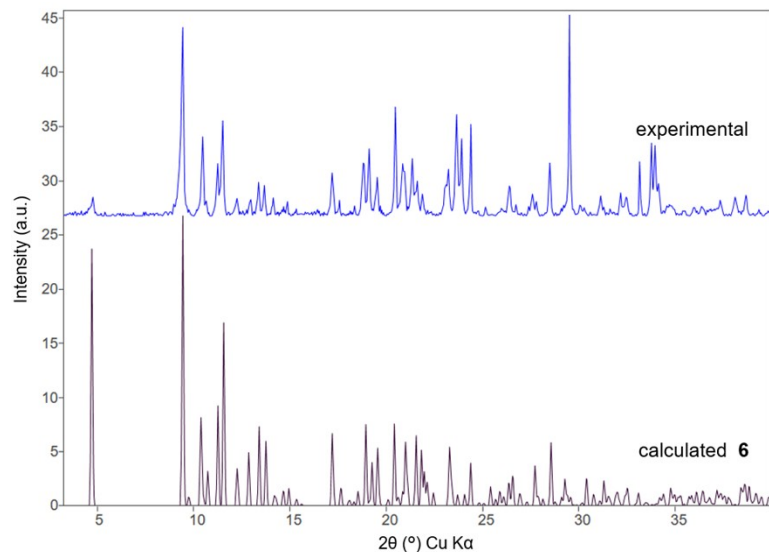


**Figure S11.** Powder X-ray diffraction data for the bulk product from which **6** was isolated. Agreement between the calculated pattern and observed pattern indicates that the crystal used for structural determination is representation of the bulk, as confirmed by element analysis.

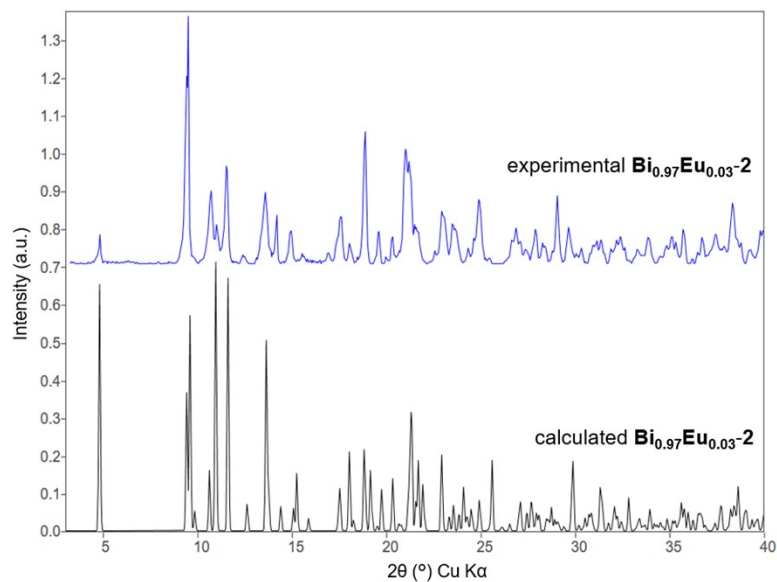


**Figure S12.** Powder X-ray diffraction data for the bulk product from which **Bi<sub>0.97</sub>Eu<sub>0.03</sub>-2** was isolated. Agreement between the calculated pattern and observed pattern indicates that the crystal used for structural determination is representation of the bulk, as confirmed by element analysis.



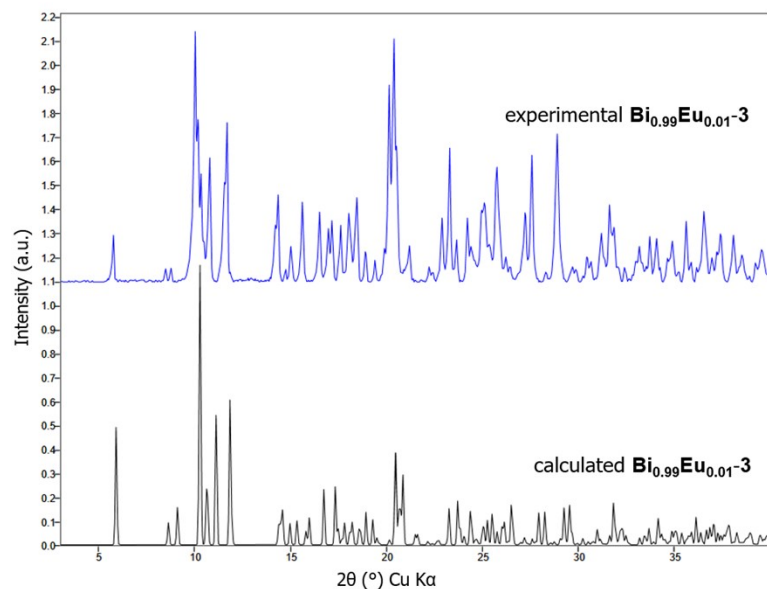


**Figure S13.** Powder X-ray diffraction data for the bulk product from which  $\text{Bi}_{0.99}\text{Eu}_{0.01-3}$  was isolated. Agreement between the calculated pattern and observed pattern indicates that the crystal used for structural determination is representation of the bulk, as confirmed by element analysis.

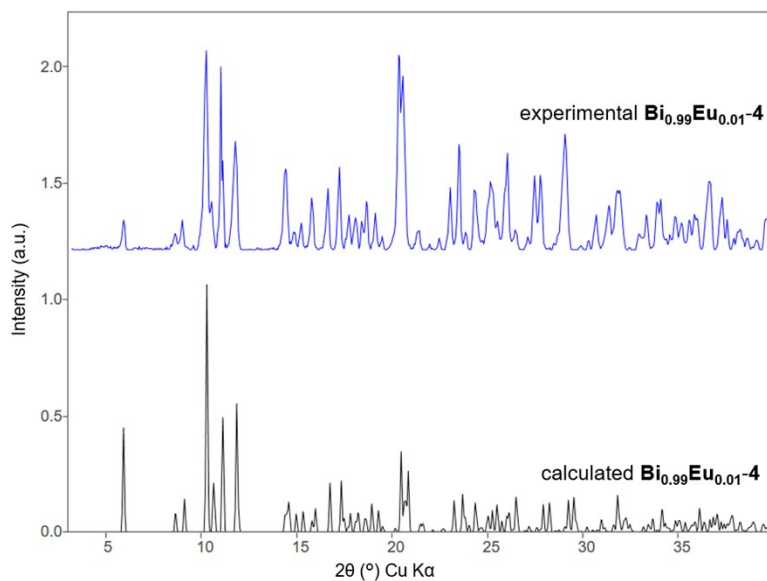


**Figure S14.** Powder X-ray diffraction data for the bulk product from which  $\text{Bi}_{0.99}\text{Eu}_{0.01-4}$  was isolated. Agreement between the calculated pattern and observed pattern indicates that the crystal used for structural determination is representation of the bulk, as confirmed by element analysis.

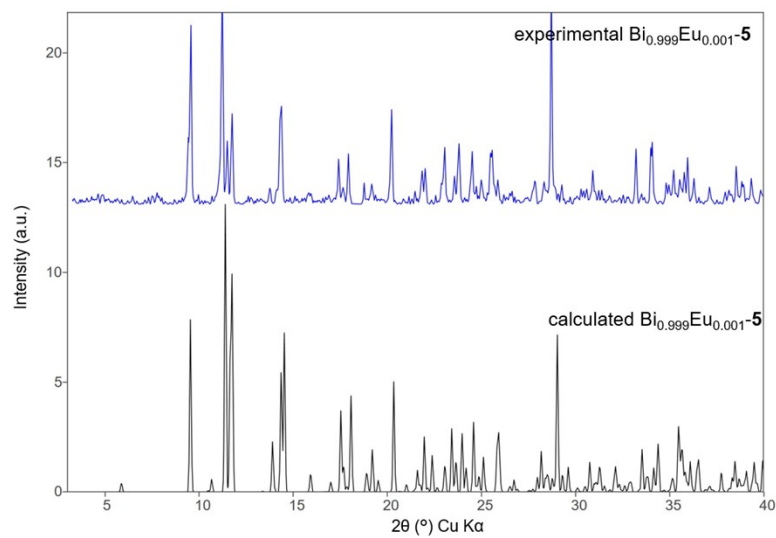


**Figure S15.** Powder X-ray diffraction data for the bulk product from which **Bi<sub>0.995</sub>Eu<sub>0.005</sub>-5** was isolated. Agreement between the calculated pattern and observed pattern indicates that the crystal used for structural determination is representation of the bulk, as confirmed by element analysis.

## Raman Spectra

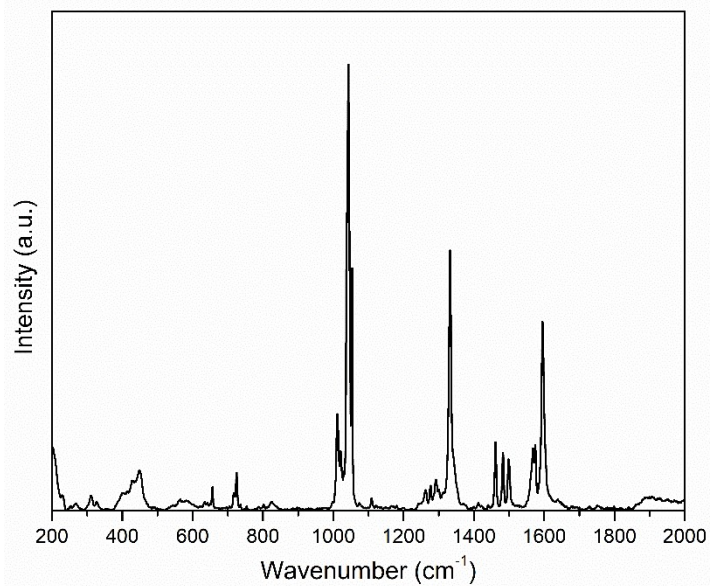


**Figure S16.** Raman spectrum for **1** shown over 200-2000 cm<sup>-1</sup>.

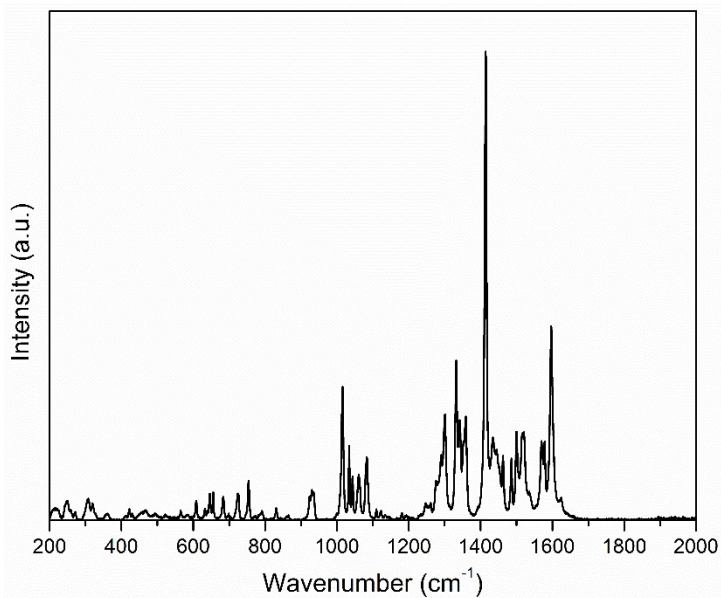


**Figure S17.** Raman spectrum for **2** shown over 200-2000 cm<sup>-1</sup>.

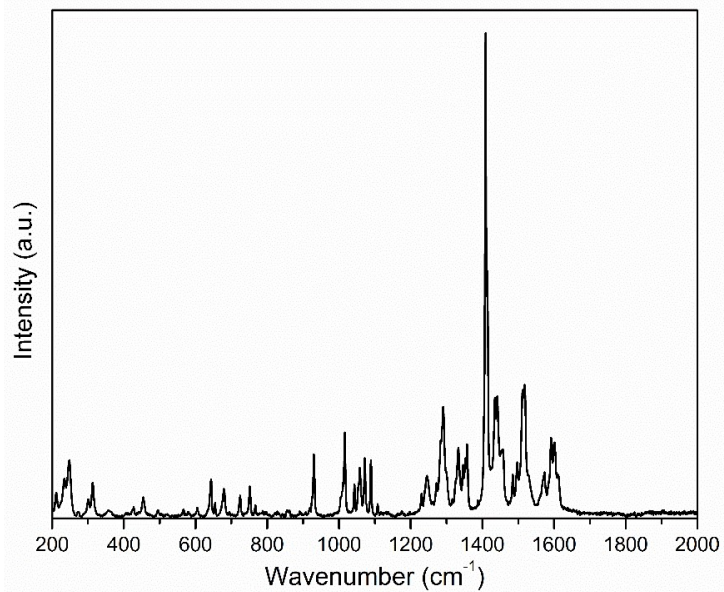


**Figure S18.** Raman spectrum for **3** shown over 200-2000 cm<sup>-1</sup>.

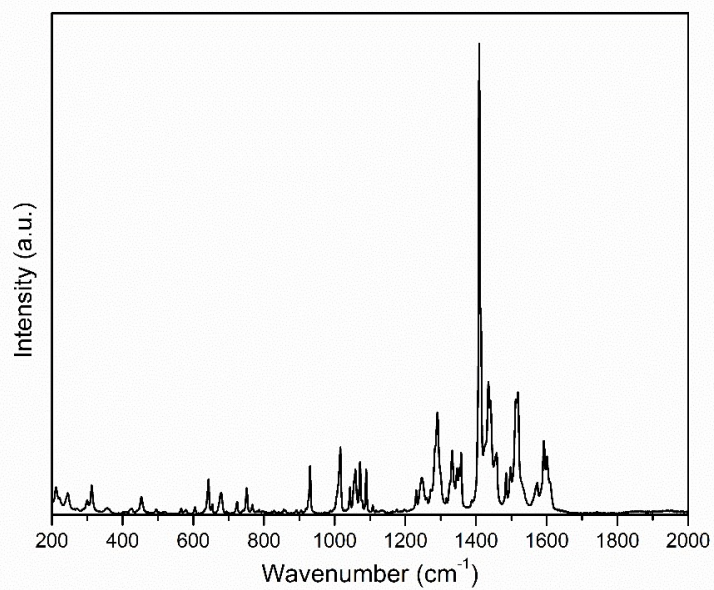


**Figure S19.** Raman spectrum for **4** shown over 200-2000 cm<sup>-1</sup>.

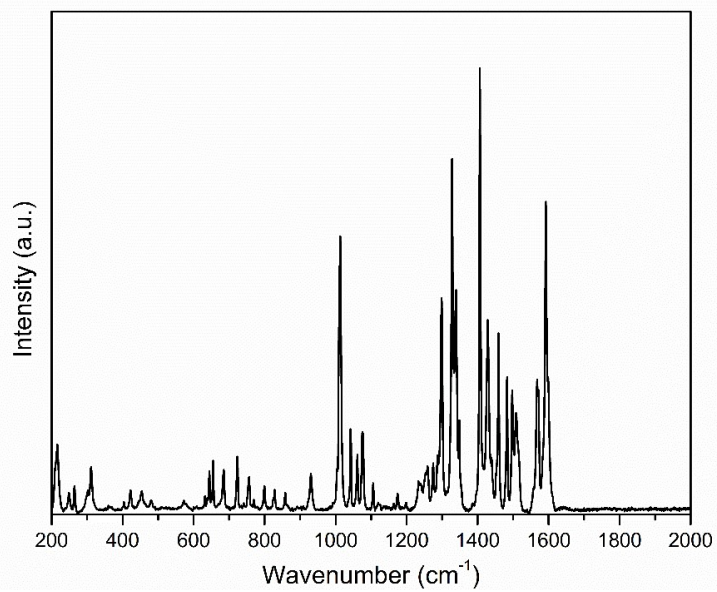


**Figure S20.** Raman spectrum for **5** shown over 200-2000 cm<sup>-1</sup>.

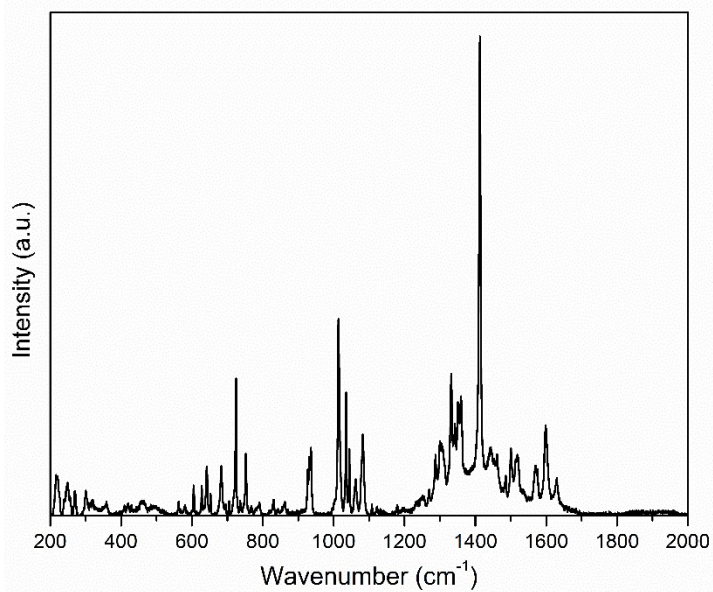


**Figure S21.** Raman spectrum for **6** shown over 200-2000 cm<sup>-1</sup>.

## Thermogravimetric Analysis

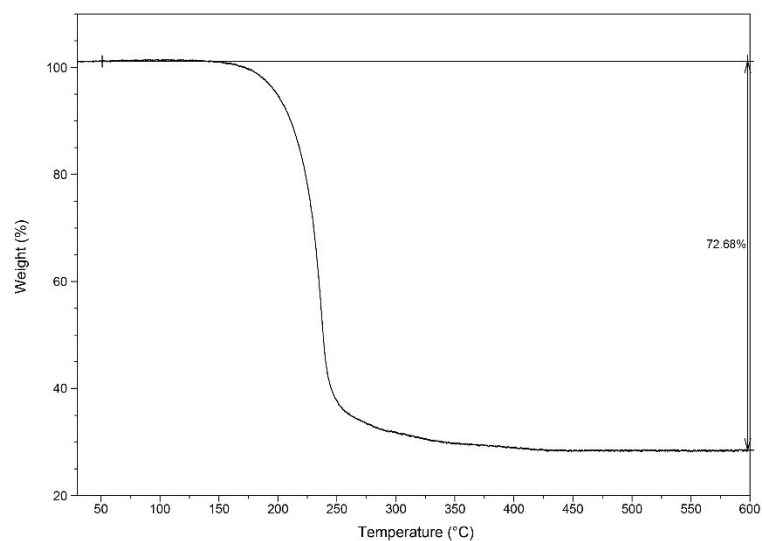


**Figure S22.** TGA plot for **2** collected over 30-600°C.

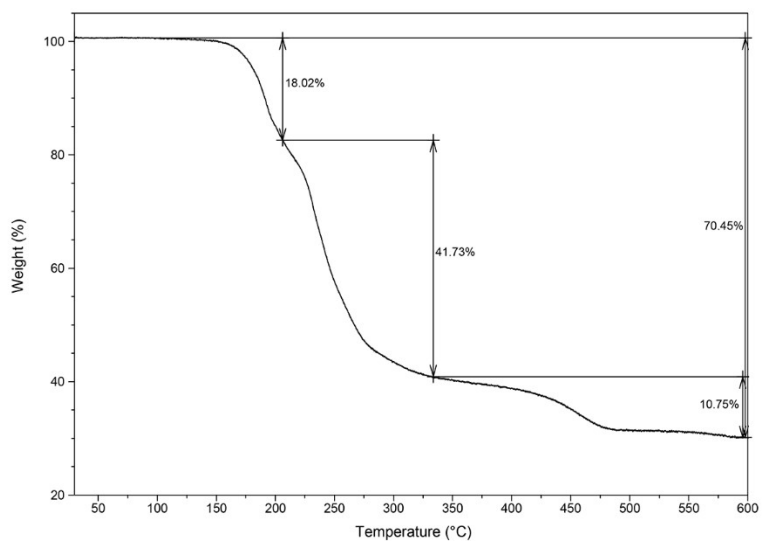


**Figure S23.** TGA plot for **3** collected over 30-600°C.

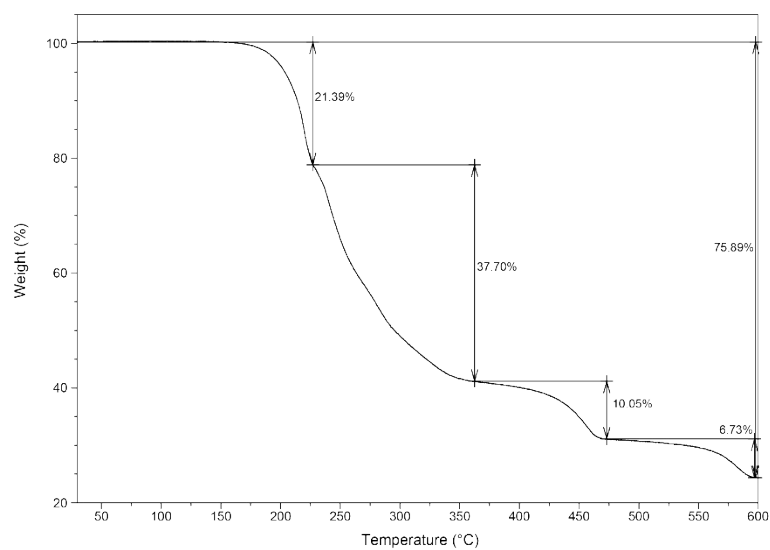


**Figure S24.** TGA plot for **4** collected over 30-600°C.

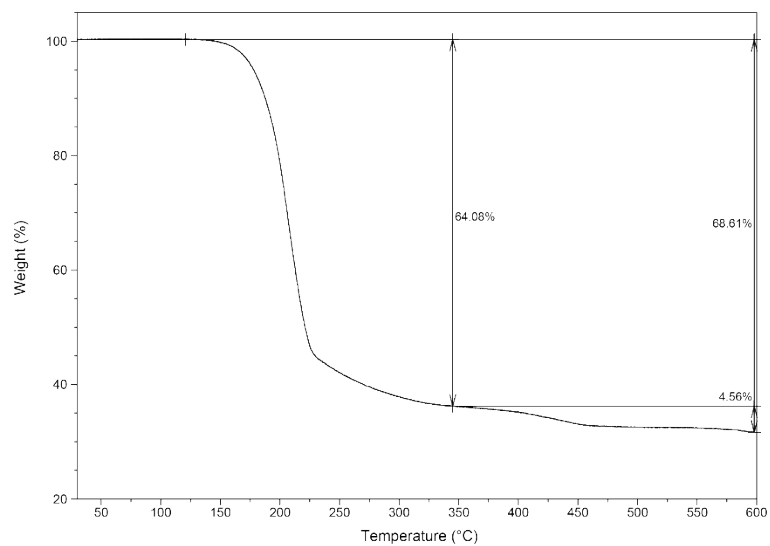


**Figure S25.** TGA plot for **5** collected over 30-600°C.

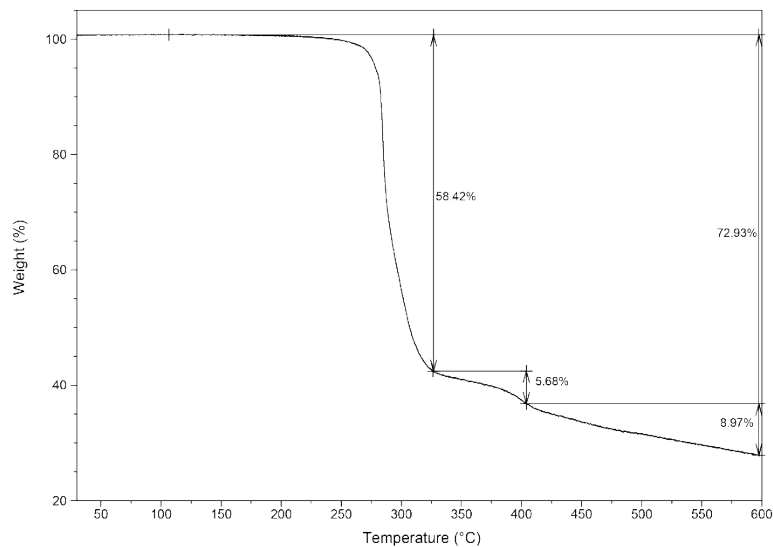


**Figure S26.** TGA plot for **6** collected over 30-600°C.

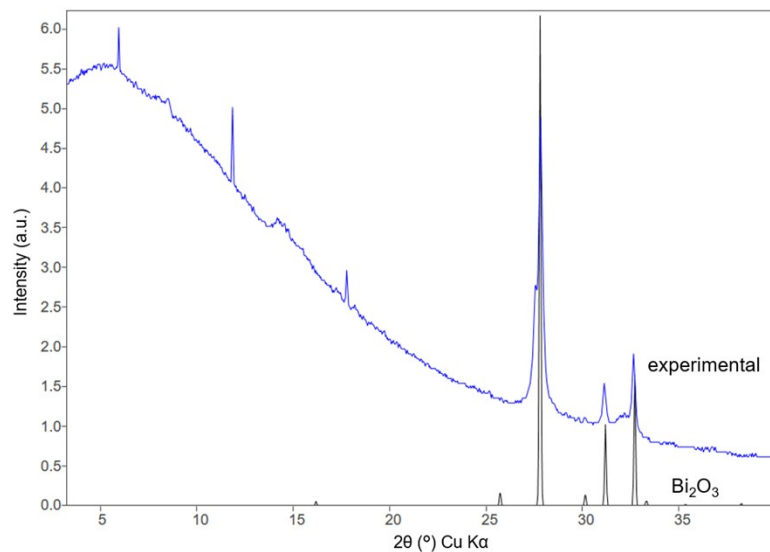


**Figure S27.** Powder X-ray diffraction data for the thermal decomposition product of **2**. The experimental peaks (blue) index well to several of the calculated peaks (black) for  $\text{Bi}_2\text{O}_3$ , though full peak assignment proved unsuccessful.



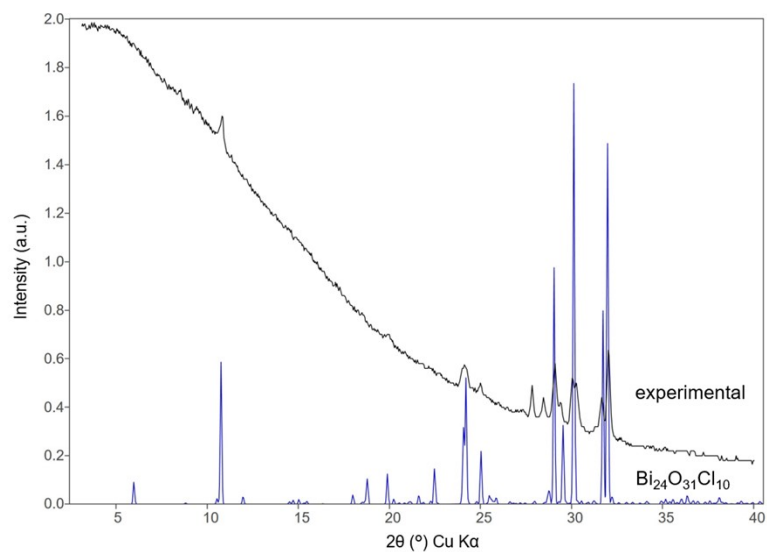


**Figure S28.** Powder X-ray diffraction data for the thermal decomposition product of **3**. The experimental peaks (black) index well to the calculated peaks (blue) for  $\text{Bi}_{24}\text{O}_{31}\text{Cl}_{10}$ .

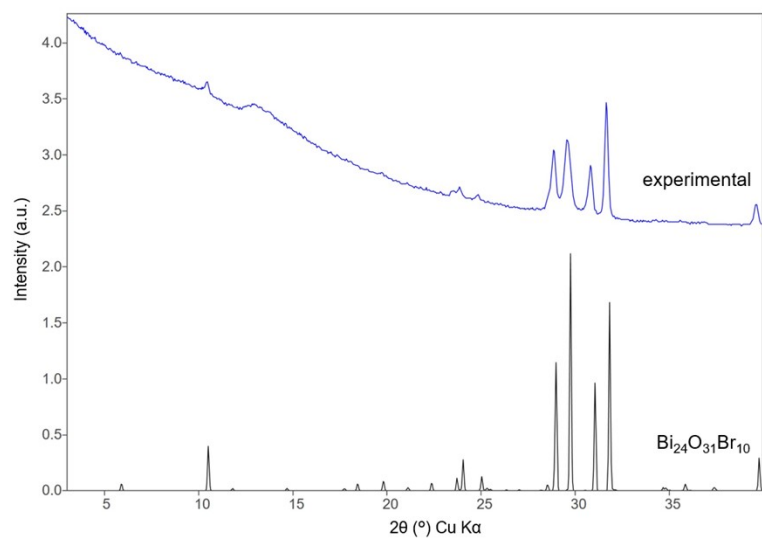


**Figure S29.** Powder X-ray diffraction data for the thermal decomposition product of **4**. The experimental peaks (blue) index well to the calculated peaks (black) for  $\text{Bi}_{24}\text{O}_{31}\text{Br}_{10}$ .

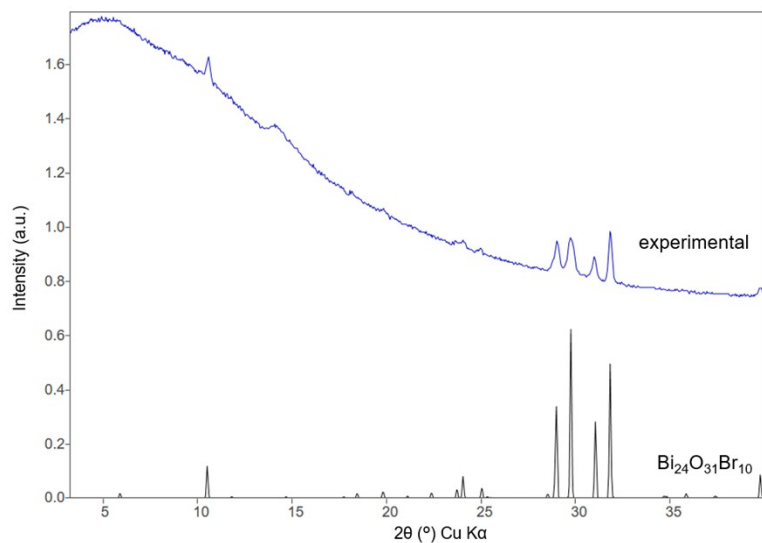


**Figure S30.** Powder X-ray diffraction data for the thermal decomposition product of **5**. The experimental peaks (blue) index well to the calculated peaks (black) for  $\text{Bi}_{24}\text{O}_{31}\text{Br}_{10}$ .

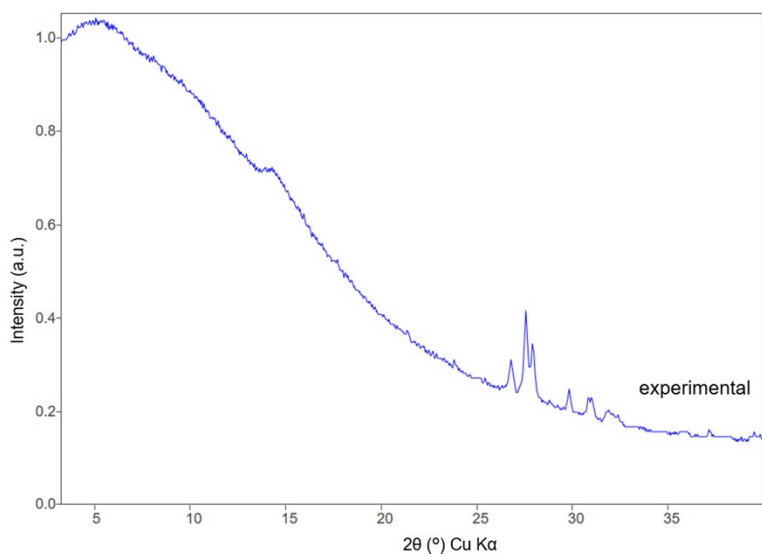


**Figure S31.** Powder X-ray diffraction data for the thermal decomposition product of **6**.

## Luminescence Measurements

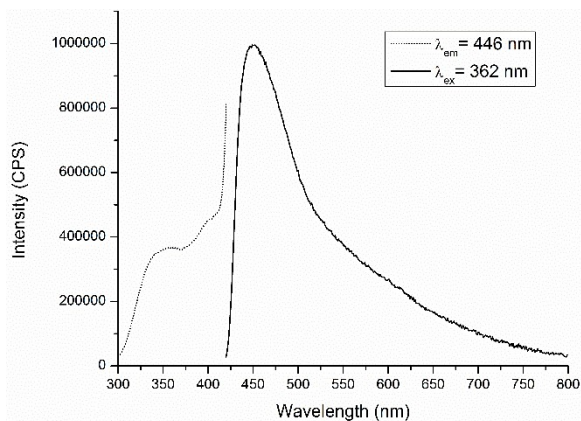


**Figure S32.** Excitation and emission spectra for 2-thenyltrifluoroacetone (TTA).

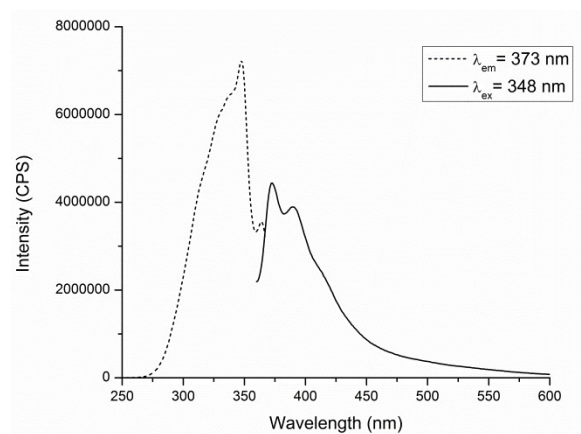


**Figure S33.** Excitation and emission spectra for 2,2';6',2''-terpyridine (terpy).

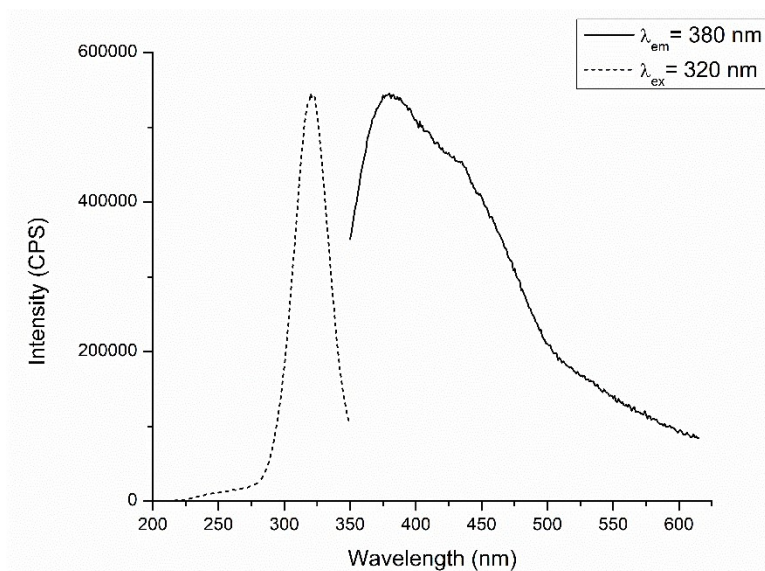


**Figure S34.** Excitation and emission spectra for **2**.

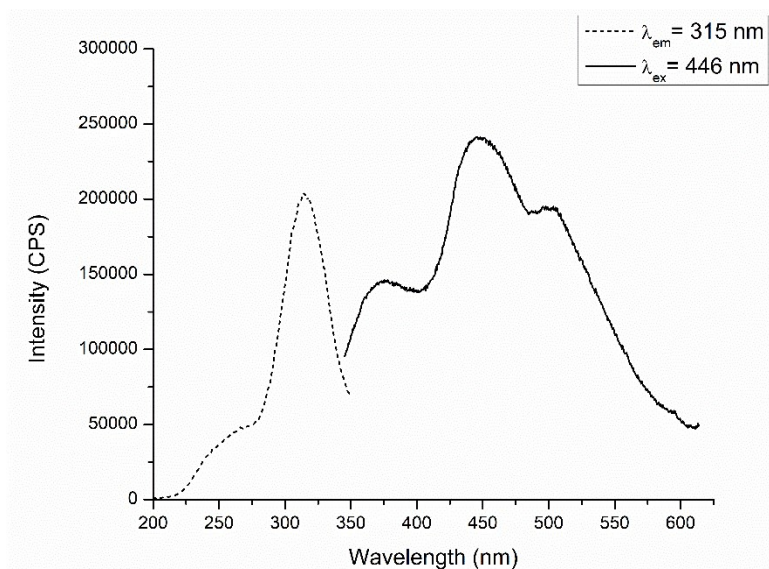


**Figure S35.** Excitation and emission spectra for 3.

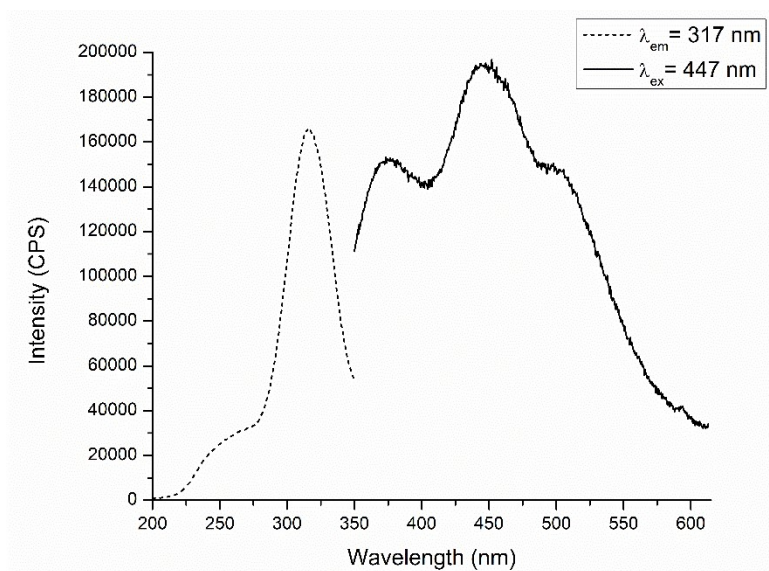


**Figure S36.** Excitation and emission spectra for 4.

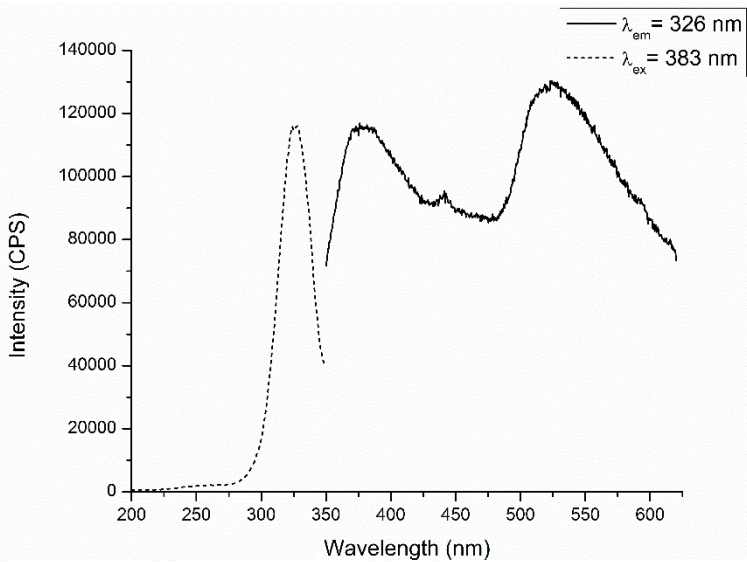


**Figure S37.** Excitation and emission spectra for **5**.

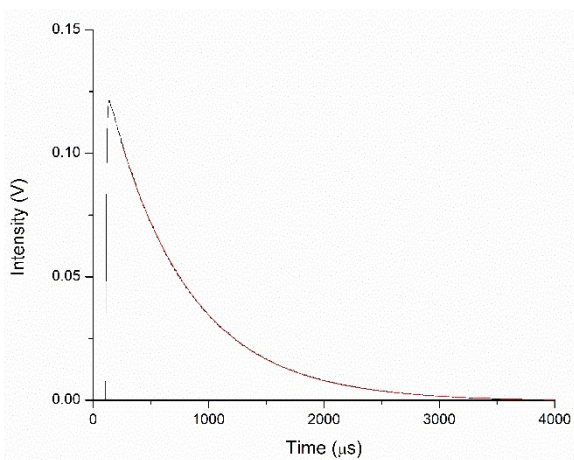


**Figure S38.** Lifetime decay curve for **Bi<sub>0.97</sub>Eu<sub>0.03</sub>-2** with the exponential decay fit plotted in red.

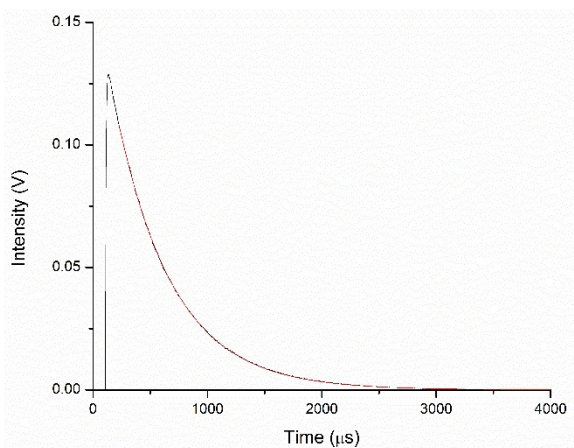


**Figure S39.** Lifetime decay curve for **Bi<sub>0.99</sub>Eu<sub>0.01</sub>-3** with the exponential decay fit plotted in red.

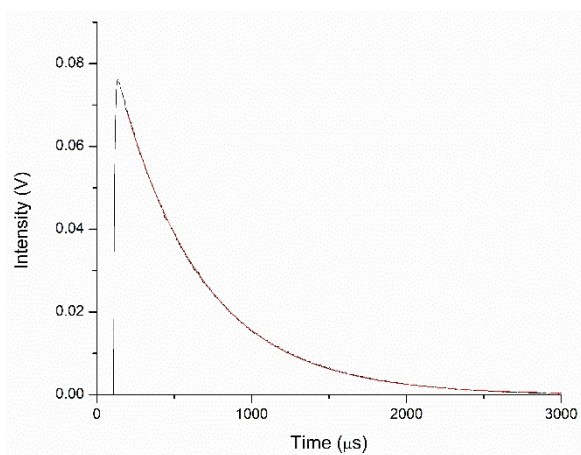


**Figure S40.** Lifetime decay curve for  $\text{Bi}_{0.99}\text{Eu}_{0.01}\text{-4}$  with the exponential decay fit plotted in red.

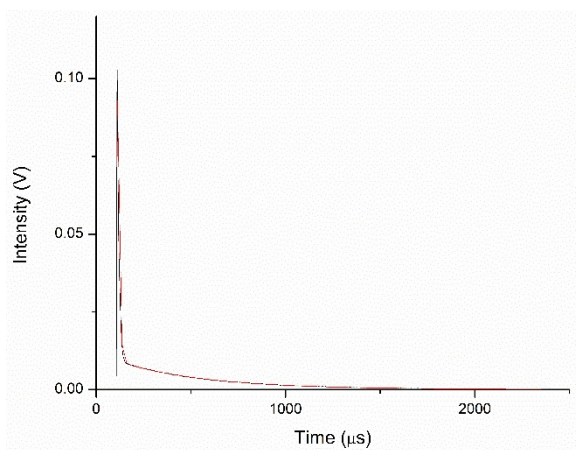


**Figure S41.** Lifetime decay curve for  $\text{Bi}_{0.999}\text{Eu}_{0.001}\text{-5}$  with the exponential decay fit plotted in red.

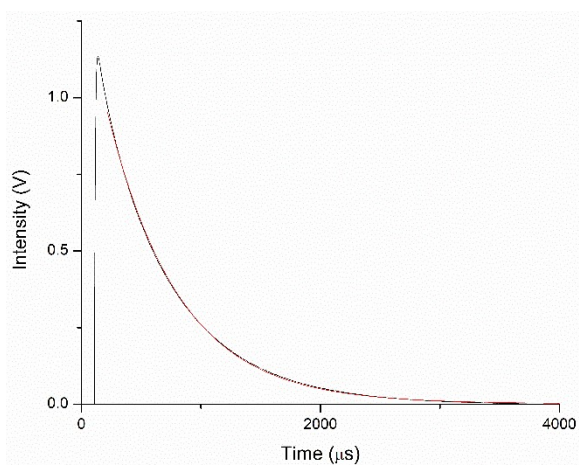


**Figure S42.** Lifetime decay curve for **6** with the exponential decay fit plotted in red.

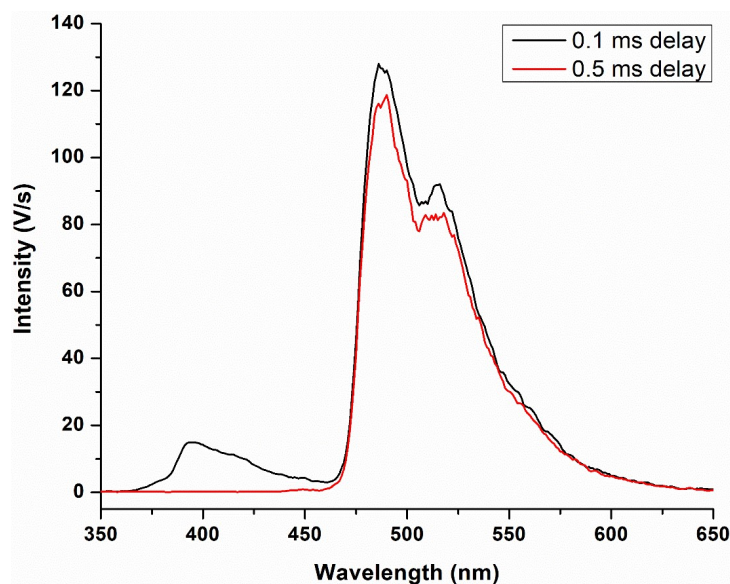


**Figure S43.** Emission spectra of the Gd-TTA complex taken at 77 K in a glass MeOH-EtOH (1:1) matrix with a time delay of 0.1 (black) and 0.5 (red) ms. Vibronic structure of the ligand is present in the spectra. The singlet state of TTA is determined from the onset of fluorescence (black), which is 374 nm ( $26,738\text{ cm}^{-1}$ ). The triplet state of TTA is determined from the onset of phosphorescence (blue), which is 465 nm ( $21,505\text{ cm}^{-1}$ ).

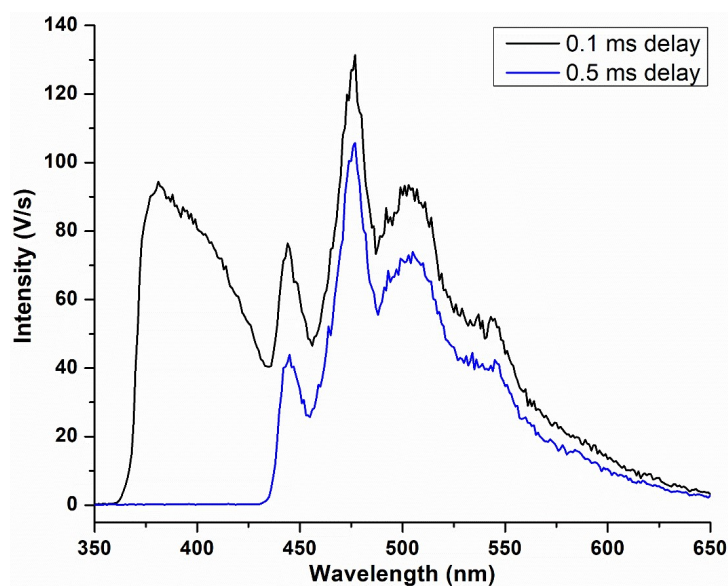


**Figure S44.** Emission spectra of the Gd-terpy complex taken at 77 K in a glass MeOH-EtOH (1:1) matrix with a time delay of 0.1 (black) and 0.5 (blue) ms. Vibronic structure of the ligand is present in the spectra. The singlet state of terpy is determined from the onset of fluorescence (black), which is 357 nm ( $28,011\text{ cm}^{-1}$ ). The triplet state of terpy is determined from the onset of phosphorescence (blue), which is 435 nm ( $22,988\text{ cm}^{-1}$ ).

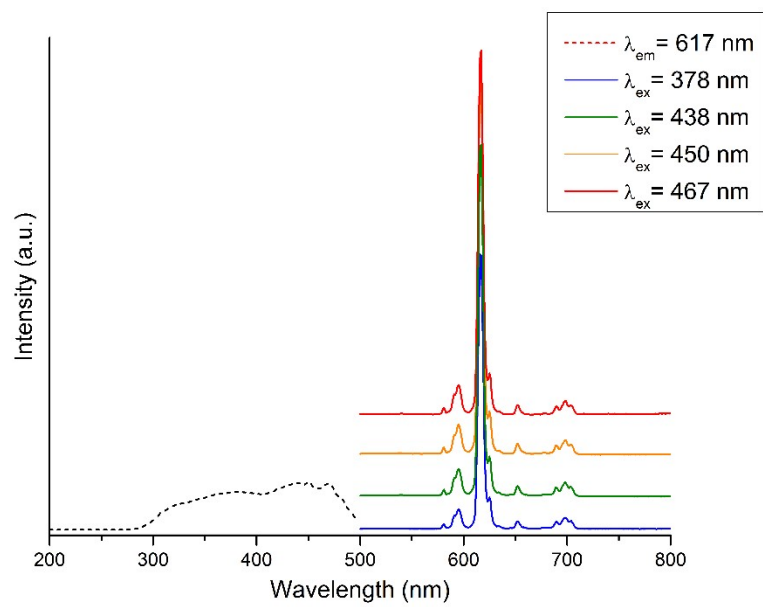


**Figure S45.** Excitation (dashed line) and emission (solid lines) of **Bi<sub>0.99</sub>Eu<sub>0.01</sub>-3** over four different excitation values.



## Summary of Potential Hydrogen Bonding Interactions in 1-6.

Table S1. C-H-Acceptor distances and angles in **1**.

<b>Donor-Acceptor</b>	<b>H ... A</b>	<b>C ... A</b>	<b>C-H ... A</b>
C12-H12 ... O23	2.53	3.178(6)	125
C12-H12 ... O31	2.50	3.370(6)	152
C14-H14 ... O33	2.54	3.162(6)	123
C19-H19 ... O31	2.36	3.276(6)	161
C113- H113 ... O21	2.53	3.137(6)	122
C114- H114 ... O22	2.46	3.386(6)	164
C115- H115 ... O32	2.48	3.113(7)	124

Table S2. C-H-Acceptor distances and angles in **2**.

<b>Donor-Acceptor</b>	<b>H ... A</b>	<b>C ... A</b>	<b>C-H ... A</b>
C17-H17 ... O41	2.34	3.257(8)	163
C18-H18 ... O43	2.55	3.246(69)	130
C27-H27A ... S31A	2.87	3.718(15)	148

Table S3. C-H-Acceptor distances and angles in **3**.

<b>Donor-Acceptor</b>	<b>H ... A</b>	<b>C ... A</b>	<b>C-H ... A</b>
C18A-H18A ... F23	2.36	3.125(10)	137
C34-H34 ... O12	2.51	3.425(4)	160
C27-H27A ... S31A	2.51	3.282(4)	138

Table S4. C-H-Acceptor distances and angles in **4**.

<b>Donor-Acceptor</b>	<b>H ... A</b>	<b>C ... A</b>	<b>C-H ... A</b>
C16-H16 ... S21B	2.83	3.606(8)	140
C28A-H28A ... F11	2.40	3.176(9)	139
C32-H32 ... F12	2.52	3.272(3)	137
C312-H312 ... O22	2.52	3.422(3)	160

Table S5. C-H-Acceptor distances and angles in **5**.

<b>Donor-Acceptor</b>	<b>H ... A</b>	<b>C ... A</b>	<b>C-H ... A</b>
C14-H14 ... Br1	2.84	3.675(3)	148
C26-H26 ... S21	2.76	3.362(3)	122
C114-H114 ... Br2	2.89	3.810(3)	162

Table S6. C-H-Acceptor distances and angles in **6**.

<b>Donor-Acceptor</b>	<b>H ... A</b>	<b>C ... A</b>	<b>C-H ... A</b>
C19-H19 ... O42	2.36	3.289(4)	166
C36A-H36A ... S21A	2.86	3.658(15)	143